Received 21 July 2019; revised 31 August 2019 and 25 September 2019; accepted 2 October 2019. Date of publication 9 October 2019; date of current version 25 October 2019. The review of this article was arranged by Editor A. G. U. Perera.

Digital Object Identifier 10.1109/JEDS.2019.2946383

A Unified Degradation Model of a-InGaZnO TFTs Under Negative Gate Bias With or Without an Illumination

SHUAI LI[1], MINGXIANG WANG[1], (Senior Member, IEEE), DONGLI ZHANG[1,2], (Member, IEEE), HUAISHENG WANG[1], AND QI SHAN[1]

1 School of Electronic and Information Engineering, Soochow University, Suzhou 215006, China
2 State Key Laboratory of ASIC and System, Fudan University, Shanghai 200433, China

CORRESPONDING AUTHOR: M. WANG (e-mail: mingxiang_wang@suda.edu.cn)

This work was supported in part by the National Natural Science Foundation of China under Grant 61574096 and Grant 61974101, and in part by the State Key Laboratory of ASIC and System, Fudan University, under Grant 2018KF006 and Grant 2019KF007.

ABSTRACT Degradation behaviors of amorphous indium–gallium–zinc–oxide (a-IGZO) thin-film transistors (TFTs) under negative bias stress (NBS) and negative bias illumination stress (NBIS) are investigated systematically. In some cases, a two-stage degradation behavior of a-IGZO TFTs is observed under both NBS and NBIS, which begins with a small positive shift of threshold voltage (V_{th}), and is followed by a large negative V_{th} shift. There is an intrinsic correlation between the degradations of NBS and NBIS. Quantitatively, both stress gate biases (V_G) and temperature dependencies of ΔV_{th} of the two degradations are found to be the same and the recovery processes are also very similar. A unified model of NBS and NBIS is proposed to consistently explain the degradation behaviors of a-IGZO TFTs and their correlation.

INDEX TERMS a-InGaZnO, thin-film transistors (TFTs), degradation, light illumination, gate bias stress.

I. INTRODUCTION

Amorphous indium–gallium–zinc–oxide (a-IGZO) thin-film transistors (TFTs) have attracted much interest for advanced displays such as active matrix organic light emitting diode (AMOLED) displays, due to their higher mobility and steeper subthreshold swing compared to a-Si TFTs [1], [2]. In practical applications, device reliability is still a critical issue for a-IGZO TFTs, namely the stability under negative bias illumination stress (NBIS) has been the focus of a lot of studies [3]–[5]. In previous works, the negative shift of the TFT threshold voltage (V_{th}) under NBIS has been attributed to holes trapping [4], where photo-excited holes injected into the gate insulator (GI) cause the negative V_{th} shift, or generation of ionized oxygen vacancies (V_O^{2+}) [5], where photo-excited V_o^{2+} traps accumulated at the interface act as the positive fixed charges. There is no attention paid to relationship between negative bias stress (NBS) and NBIS degradation in literatures.

In this study, instabilities of a-IGZO TFTs under both NBS and NBIS are investigated for different stress gate biases (V_G), temperatures (T) and light intensities (I) systematically. Besides the normally observed continuous negative V_{th} shift of TFTs, a two-stage degradation behavior, which begins with an initial positive V_{th} shift first before the normal degradation, is also observed in some TFTs. Interestingly, NBS and NBIS degradations show an intrinsic correlation including their recovery, irrespective of single- or two- stage degradation occurring in TFTs. To explain such correlation, as well as the degradation behaviors of both NBS and NBIS instabilities, a unified model is proposed based on the generation of negative charges and V_O^{2+} at the channel/ GI interface respectively for the positive and negative V_{th} shift. On this basis, the NBS and NBIS degradation of a-IGZO TFTs can be understood with the same mechanisms for the first time.

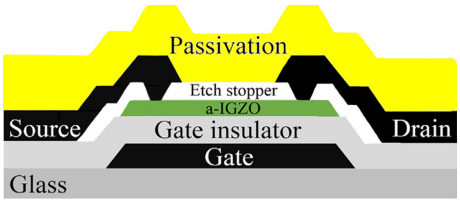

FIGURE 1. Schematic cross section of the a-IGZO TFT with an inverted staggered bottom gate structure.

II. EXPERIMENTAL

Inverted staggered bottom gate a-IGZO TFTs were fabricated on glass substrates, as shown in Fig. 1. For sample type A, a 100 nm thick Mo gate electrode was sputtered, and 120 nm gate oxide (SiO_2) layer was deposited by plasma-enhanced chemical vapor deposition (PECVD) at 300 °C. Then, 50 nm thick a-IGZO channel layer was deposited by RF magnetron sputtering at room temperature. A 50 nm thick PECVD SiO_2 was used as the etching stop layer (ESL). The contact holes were opened by dry etching and the source/drain (S/D) electrodes were sputtered. Finally, 100 nm SiN_x passivation layer was deposited. TFTs were annealed at 350 °C for 1h in air. For sample type B, the process is similar to sample A. Only differences are that the ESL thickness is thicker (100 nm), and there is no passivation layer. Both types are typical a-IGZO TFTs. Device channel length (L) and width (W) are 20 and 10 μm, respectively. The TFT samples have been stored in our laboratory in a controlled ambient (22 °C, humidity of 18%) for months, after their fabrication and before the stress tests. Systematic NBS or NBIS tests with different stress V_G, T and I were carried out mainly on samples type A. Selected tests were performed on sample type B for verification and supplement. For all stress tests, S and D were grounded. Illumination was conducted by an LED light with a wavelength of 445 nm. IV curves were measured at drain bias V_D of 5 V in dark by using Agilent 4156C semiconductor parameter analyzer. Device V_{th} was defined as the V_G where drain current I_D reached 10 nA.

III. RESULTS AND DISCUSSIONS

A. NBIS DEGRADATION

Shown in Fig. 2 is the evolution of the transfer curve of a type A TFT under NBIS of $V_G = -30$ V and $I = 1$ mW/cm^2 for 3000 s at 20 °C. Its initial characteristics V_{th} of 3.64 V, subthreshold swing (SS) of 0.3 V/dec, and field-effect mobility (μ_{FE}) of 18.2 cm^{2}V^{-1}s^{-1} are typical. Different from commonly observed negative V_{th} shift [4], [5], a two-stage NBIS degradation is observed. In the first-stage within 100 s, V_{th} shifts positively for 1.0 V. Then, a turnaround occurs and V_{th} begins to shift negatively. V_{th} shift (ΔV_{th}) is −3.47 V at 3000 s.

Fig. 3 shows the time dependence of ΔV_{th} under NBIS of different V_G with fixed $I = 1$ mW/cm^2 for 3000 s at 20 °C. It is seen that V_{th} degradation in both stages is enhanced at higher stress V_G, i.e., V_{th} in the first stage shifts more positively, whereas in the second stage, it drops more negatively. At lower V_G, the highlighted turnaround occurs earlier, suggesting that the 1st-stage degradation is more sensitive to the stress V_G.

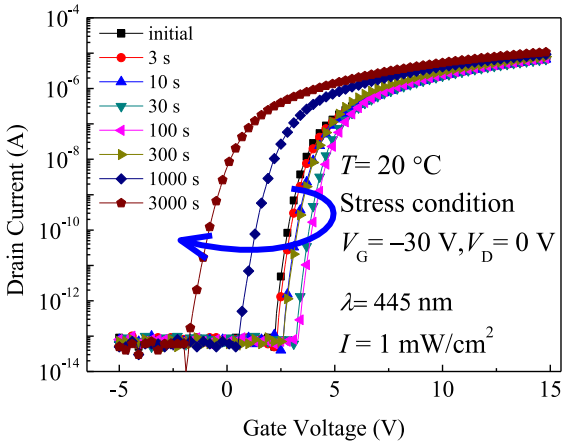

FIGURE 2. The transfer curves of the a-IGZO TFT under NBIS for $V_G = -30$ V, $I = 1$ mW/cm^2.

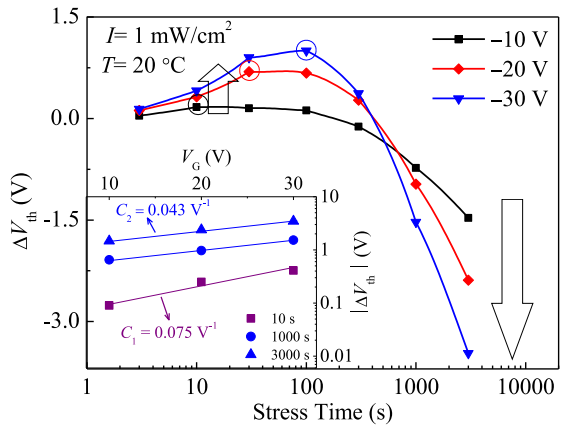

FIGURE 3. Stress time dependence of ΔV_{th} under NBIS for different V_G (inset) extracted C_1 and C_2 in two stages.

In the negative bias temperature instability (NBTI) of MOSFETs and poly-Si TFTs, device degradation follows [6], [7] the relationship:

$$\Delta V_{th} \propto t^n \exp(-E_a/\mathrm{kT}) \exp(CV_G) \quad (1)$$

ΔV_{th} follows a power law dependence on stress time, with a time exponent n, the Arrhenius dependence on T with an activation energy E_a, and an exponential dependence on stress V_G with a characterizing parameter C [6]–[8]. For a-IGZO TFTs, previous studies show that the negative V_{th} shift of NBIS increases with V_G, due to larger vertical electric field within the channel [5], [9]. In this study, it is found that the degradation in both stages follows the same V_G dependence as in Eq. (1). As plotted in the inset, parameter C_1 is 0.075 V^{-1} for the 1st-stage and C_2 is 0.043 V^{-1} for the 2nd-stage.

Fig. 4 shows the time dependence of ΔV_{th} under NBIS of different Ts at fixed $V_G = -20$ V and $I = 1$ mW/cm^2

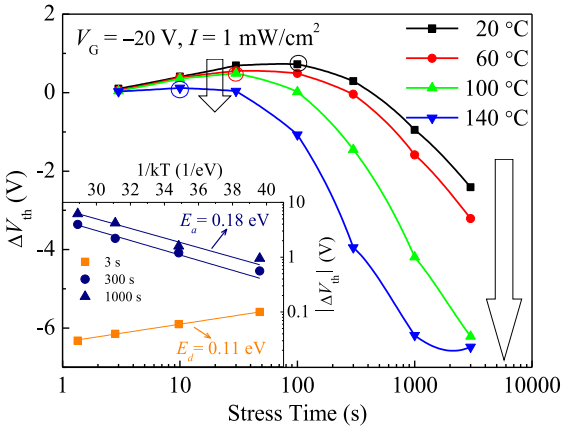

FIGURE 4. Stress time dependence of ΔV_{th} under NBIS at different temperatures (inset) extracted E_d and E_a in two stages.

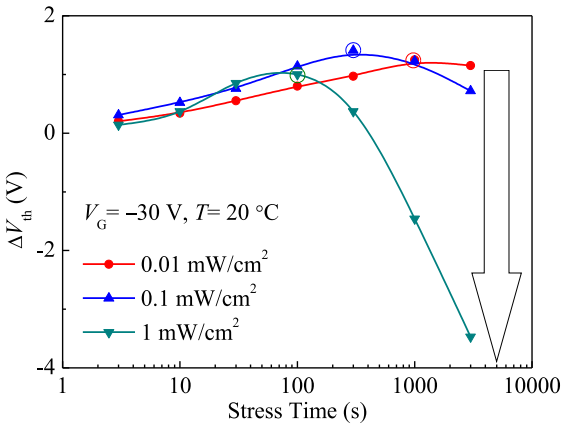

FIGURE 5. Stress time dependence of ΔV_{th} under NBIS with different light intensities.

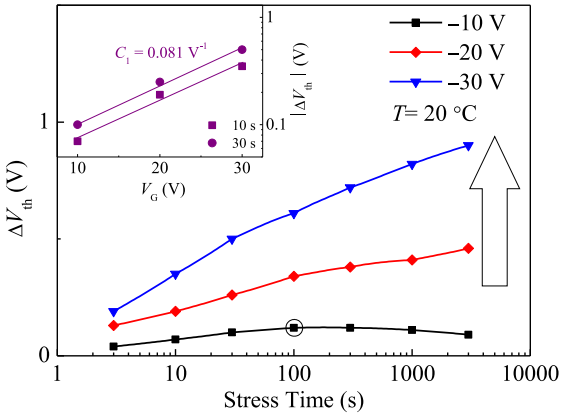

FIGURE 6. Stress time dependence of ΔV_{th} under NBS for different V_G (inset) extracted C for the first-stage.

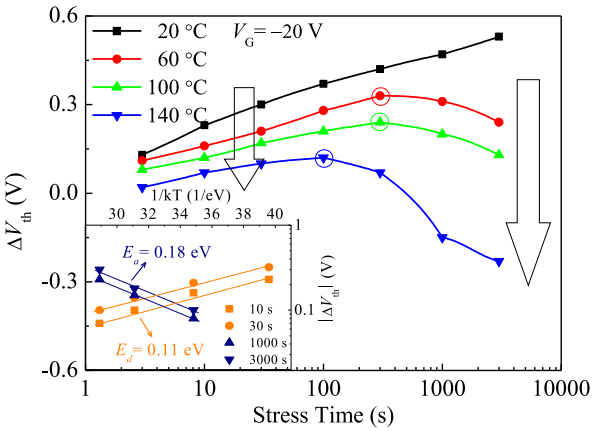

FIGURE 7. Stress time dependence of ΔV_{th} under NBS at different temperatures (inset) extracted E_d and E_a in two stages.

for 3000 s. It is seen that, at elevated T, the positive V_{th} shift in the 1st-stage is suppressed, whereas the negative V_{th} shift in the 2nd-stage is enhanced. As shown in the inset, the negative V_{th} shift in the 2nd-stage follows the Arrhenius relationship with T and E_a is extracted to be 0.18 eV. While the positive V_{th} shift in the 1st-stage also follows a similar dependency, but with a *de*-activation energy (E_d) of 0.11 eV.

Fig. 5 shows the time dependence of ΔV_{th} under NBIS of different Is from 0.01 to 1 mW/cm^2 at fixed $V_G = -30$ V, 20 °C. One sees that the 2nd-stage degradation occurs earlier and becomes more severe as I increases. However, the positive V_{th} shift in the 1st-stage is insensitive to the light illumination. For example, at 100 s ΔV_{th} are 0.8, 1.14, and 1 V, respectively for I = 0.01, 0.1, and 1 mW/cm^2. Light intensity increases 100 times, but the positive V_{th} shifts in the 1st-stage are similar.

From Fig. 2-5, one notes that the two-stage NBIS degradation behavior consistently appears under different V_G, T, and I conditions. The 1st-stage positive V_{th} shift would be more obvious at higher V_G and lower T conditions. This is apparently different from previous observations for NBIS [4], [5], where only the negative V_{th} shift was reported.

B. NBS DEGRADATION

In order to clarify the mechanisms of the two-stage degradation of a-IGZO TFTs under NBIS, NBS tests without an illumination are also conducted on type A samples under different V_G and Ts. Shown in Fig. 6 is the time dependence of ΔV_{th} under NBS of different V_G at 20 °C for 3000 s. It can be seen that V_{th} shifts positively and the positive V_{th} shift is enhanced at higher V_G. Based on Eq. (1), the parameter characterizing the V_G dependency C_1 is extracted to be 0.081 V^{-1} as shown in the inset, which is close to that of the 1st-stage NBIS degradation in Fig. 3 0.075 V^{-1}. At lower $V_G = -10$ V, the positive V_{th} shift becomes smaller and one notes that the two-stage degradation behavior appears in NBS.

Fig. 7 shows the time dependence of ΔV_{th} under NBS of different Ts at fixed $V_G = -20$ V for 3000 s. It is seen that the two-stage degradation becomes more obvious as T rises. At elevated Ts, ΔV_{th} of the 1st-stage is suppressed while the 2nd-stage degradation occurs earlier and more significantly. Such T dependence of NBS is the same as that of NBIS, i.e., the positive V_{th} shift of the 1st-stage suppressed, whereas the 2nd-stage enhanced by T. The extracted E_d and E_a are

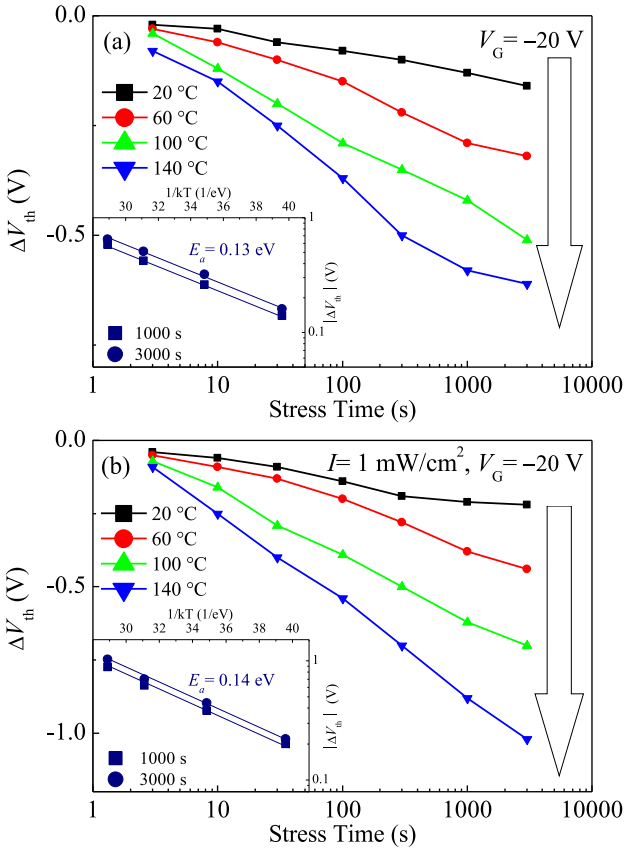

FIGURE 8. Stress time dependence of ΔV_{th} under (a) NBS, (b) NBIS at different temperatures for type B samples (inset) extracted E_a for NBS and NBIS, respectively.

0.11 eV and 0.18 eV respectively for the 1st and 2nd-stage degradation.

Comparing the NBS (Fig. 7) and NBIS (Fig. 4) degradation under the same stress V_G conditions, it is apparent that NBIS enters the 2nd-stage much earlier, and the negative V_{th} shift of the 2nd-stage is significantly aggravated. However, one notes that both E_d and E_a values of NBS equal to those of NBIS, respectively. Since the two-stage degradation behaviors under NBS and NBIS are similar, more importantly, their V_G dependency characterized by C_1, and T dependency characterized by E_d and E_a respectively for the 1st and 2nd -degradation stage, are also the same. It strongly suggests that there should be some intrinsic correlation between the NBS and NBIS degradation.

C. MORE EVIDENCES ON TYPE B SAMPLES

In order to confirm the above observations, we choose to conduct NBS and NBIS tests again on samples with different fabrication process. Type B samples have different ESL thickness and have no SiN_x passivation. Their characteristics V_{th}, SS, and μ_{FE} of 0.9 V, 0.26 V/dec, and 17.8 cm^2 V^{-1} s^{-1}, respectively are also typical for a-IGZO TFTs.

TABLE 1. Extracted V_G dependency (C), E_d, E_a under NBS and NBIS.

Samples	First-stage				Second-stage	
	NBS E_d (eV)	NBIS E_d (eV)	NBS C_1 (V^{-1})	NBIS C_1 (V^{-1})	NBS E_a (eV)	NBIS E_a (eV)
A	0.11	0.11	0.075	0.081	0.18	0.18
B	—				0.13	0.14

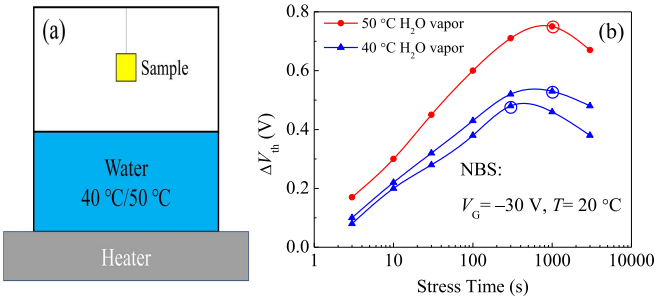

FIGURE 9. (a) Schematic illustration of experiments for sample B in humid ambient. (b) Stress time dependence of ΔV_{th} under NBS for sample B.

Fig. 8 (a) and (b) show the time dependence of ΔV_{th} under NBS and NBIS respectively, at different Ts with fixed $V_G = -20$ V. It is seen that both degradations have a continuous negative V_{th} shift, which is similar to previous observations [4], [5], whereas different from the two-stage degradation of type A sample. Nevertheless, both degradations are still correlated. Within expectation, the negative V_{th} shift is thermally activated, and the extracted E_a are 0.13 and 0.14 eV, respectively for NBS and NBIS, which are almost the same.

To further convince that the H_2O effect for sample B is eliminated after annealing, additional experiments have been carried out for sample B. First, as shown in Fig. 9 (a), sample B is suspended in a bottle with some water for 0.5 h, and the temperature is kept at 40 °C (2 samples) or 50 °C (1 sample). Without SiN_x passivation, moisture in humid ambient will be absorbed into TFTs. Then NBS of $V_G = -30$ V for 3000 s is performed on three TFTs. The V_{th} degradation under NBS is shown in Fig. 9 (b). Similar to the degradation phenomena of sample A under NBS, a two-stage degradation, where a positive V_{th} shift followed by a negative shift is observed. Moreover, the higher the vapor temperature is, where more H_2O is diffused into the TFTs, the larger positive V_{th} shifts and the longer the first stage appears.

For sample A, we performed the NBS of $V_G = -30$ V, $T = 20$ °C for 1000 s. For sample B, we performed the same NBS or NBIS of the same V_G with $I = 1$ mW/cm^2. As shown in Fig. 10(a)-(c), after 1000 s stress positive ΔV_{th} of 0.82 V, negative ΔV_{th} of 0.48 V and 0.62 V appears respectively. Then the recovery is observed in the dark after stress removal. As shown in Fig. 10 (d)-(f), the NBS recovery of sample A is quite different from that of sample B. The positive V_{th} degradation of sample A can fully recover

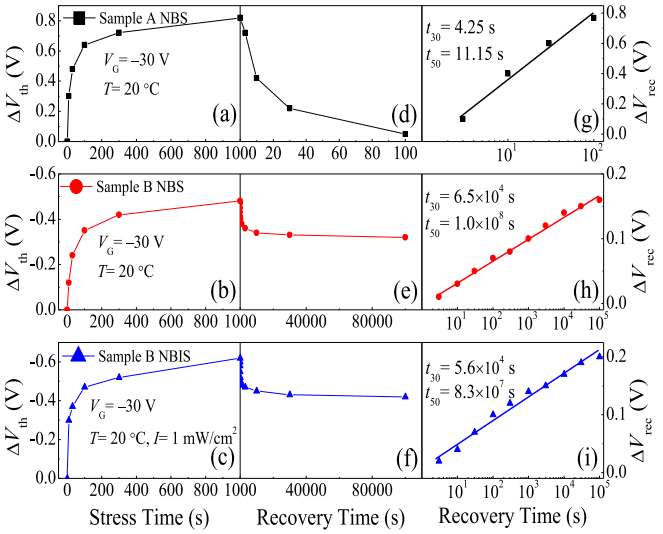

FIGURE 10. **(a)-(c) Stress time dependence of ΔV_{th} for sample A under NBS, sample B under NBS, sample B under NBIS, respectively. (d)-(f) and (g)-(i) Recovery time dependence of ΔV_{rec} for sample A under NBS, sample B under NBS, sample B under NBIS in linear and logarithmic time scales, respectively.**

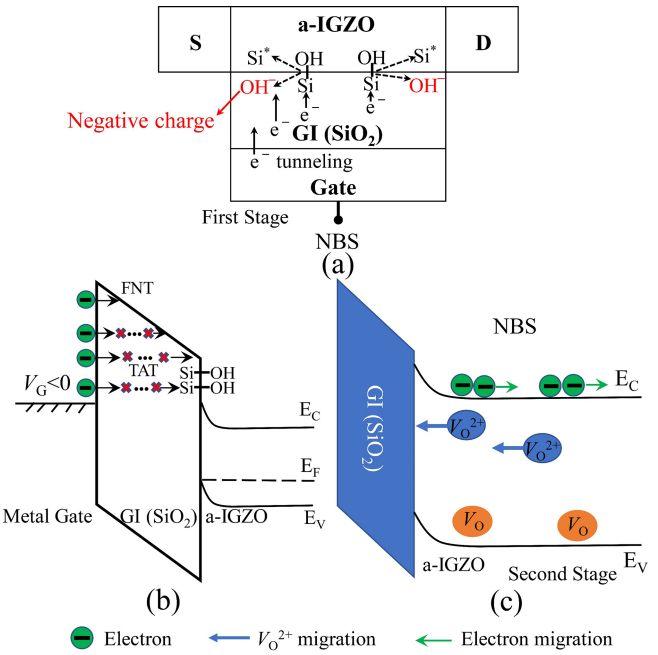

FIGURE 11. **(a) Schematic illustration of physical model in the first-stage degradation under NBS or NBIS. (b) Schematic energy band diagram for electron tunneling in the first-stage degradation under NBS. (c) Energy band diagram illustrating the second-stage degradation under NBS.**

within 100 s, while sample B takes 1.0×10^6 s to recover only ~33.3 % of the initial amount of negative V_{th} degradation under NBS. Furthermore, it is interesting to find that the recovery of NBIS is quite similar. It takes 1.0×10^6 s for sample B to recover ~32.3 % of the initial amount of negative V_{th} degradation under NBIS. As shown in Fig. 10 (g)-(i), the amount V_{th} shift caused by recovery ΔV_{rec} of all samples follows a logarithmic dependence on the recovery time, from which we can extract the characteristic recovery time t_{30} and t_{50}, which is the time required to recover 30% and 50% of the initial amount of degradation. All values are listed in the corresponding figures for comparison. One notes that, t_{30} and t_{50} for the negative V_{th} degradation under both NBS and NBIS for sample B are quite close, but are orders of magnitudes longer than the recovery times of the positive V_{th} degradation of NBS for sample A. It clearly suggests the same mechanism involved for the negative V_{th} degradation of both NBS and NBIS instabilities, while totally different mechanisms for the positive and negative V_{th} degradation under NBS instability.

Based on above observations, it is confirmed that the NBS and NBIS degradation of a-IGZO TFTs are indeed correlated, whether V_{th} following the single or two-stage degradation behaviors, although the amount of negative V_{th} degradation of NBIS is much larger than that of NBS under same V_G and T. Furthermore, the V_G and T dependencies of ΔV_{th} for NBS and NBIS degradation are also the same as observed on TFTs with different fabrication process. As summarized in Table 1, all characterizing parameters extracted from both type A and B samples for NBS and NBIS degradations are nearly the same. It strongly suggests that the underlying degradation mechanisms of two kinds of degradation should be unified.

IV. A UNIFIED DEGRADATION MODEL OF NBS AND NBIS

A. NBS

For the positive V_{th} shift of NBS degradation in a-IGZO TFTs, previous study attributed it to charge trapping into the gate insulator (GI) or at the channel/GI interface [10], [11]. However, there was no detailed mechanisms mentioned. Note type A sample has a passivation of SiN_x. It is reported that there is a high hydrogen concentration in SiN_x layer and hydrogen can diffuse into the channel. As an impurity in the a-IGZO channel, it can affect the electrical properties of a-IGZO TFTs [12], [13]. However, the role of hydrogen is mainly understood as a shallow donor of a-IGZO channel, which increases the amount of free electrons. On this basis, more hydrogen diffusion into the channel will turn on the TFT earlier, or induces a negative V_{th} shift, which is in contrary to the positive V_{th} shift as observed in the 1st-stage degradation. Thus, the effect of hydrogen is insignificant. Here, we propose that some residual water (H_2O) molecules unintentionally introduced from fabrication processes may accumulate at the channel/GI interface and react with SiO_2 to form immobile Si hydroxyl groups [8], [14], as shown in Fig. 11 (a), i.e.,

$$H_2O + \equiv Si - O - Si \equiv \longleftrightarrow \equiv Si - OH + OH - Si \equiv \quad (2)$$

In the presence of an electric field induced by NBS, some gate electrons can get into the GI via a number of trap assisted tunneling (TAT) [15] and/or Fowler-Nordheim tunneling [16], as shown in Fig. 11 (b), since the GI is PECVD SiO_2 which is relatively thick and defective. Negative charges formation is usually not likely to occur

without the effect of water vapor [17] and a small fraction of electron trapping within the bulk of the GI could be negligible. At the interface, some of the tunneling electrons can be captured by the neutral OH-Si= traps to form the negative OH^- charges:

$$e^- + \equiv \mathrm{SiOH} \longleftrightarrow \equiv \mathrm{Si}^* + \mathrm{OH}^- \tag{3}$$

which leads to the positive V_{th} shift. Here the charge trapping model is similar to previous ones for MOSFETs [17] or poly-Si TFTs [18]. However, the 1st-stage won't last long, because at the interface the amount of H_2O molecules and $\mathrm{Si-OH}$ bonds are limited. Our model is consistent with previous observations that moisture can cause V_{th} shift in poly-Si and a-IGZO TFTs [19], [20].

The 1st-stage degradation occurs only in part of the a-IGZO TFTs, which is thought to be affected by some moisture unintentionally introduced during the fabrication process before SiN_x passivation layer is covered. For type A sample, once the passivation is done, it can be hardly affected by the moisture in the ambient. Since the SiN_x passivation layer is a good barrier to block water vapor [21], [22], even with a thermal annealing, the residual H_2O molecules still cannot escape from the device. While for type B sample without a SiN_x passivation, the residual H_2O molecules could be removed during the annealing process. Thus, type B sample has no H_2O effect.

Under larger stress V_G or electric field within the GI, the reaction (3) is more active to produce more OH^- ions, which causes larger V_{th} shift. While at higher T, it turns out that the initially aggregated H_2O molecules at the channel/GI interface tend to spread out into nearby vicinities. In other words, the spatial distribution of H_2O molecules becomes more dispersive, so that the amount of OH^- ions that could be generated at the interface is reduced. Thus, the 1st-stage degradation is suppressed by elevated T.

To understand the quick recovery for positive ΔV_{th} under NBS or NBIS, it is suggested that once NBS or NBIS is removed, the reaction (3), which generates OH^- ions, will stop. During the recovery phase, where both the vertical electric field within the GI and channel electrons are absent, the inversed reaction becomes effective. Limited amount of OH^- ions are quickly consumed hence the positive V_{th} degradation recovers in a short time.

It is known that V_O plays an important role in oxide TFTs [5], [9]. Most V_O defects have deep donor levels, while in some cases, where the neighboring metal atoms are strongly back-bonded to the second neighboring O atoms, an outward relaxation takes place, resulting in spontaneous ionization of V_O, i.e., V_O^{2+} [23]. Besides, V_O^{2+} can be also formed by thermal excitation [9]. Hence, the a-IGZO channel naturally contains some V_O^{2+}. It's important to note that although V_O^{2+} states in a-IGZO can capture electrons and returns to neutral V_O, they are relatively stable because the neighboring metal atoms would undergo outward relaxation, which forms an energy barrier (E_B) to hinder V_O^{2+} return to V_O [24], [25].

For the 2nd-stage degradation, with the presence of a negative V_G, channel electrons would accumulate to the back channel. The balance between the concentrations of V_O^{2+} and electrons must be re-established. More V_O^{2+} would be annihilated at the place where electrons accumulated, and more V_O^{2+} would be generated at the place where electrons departed from. Such a re-balance results in a concentration gradient of V_O^{2+} within the channel, which is equivalent to the movement of V_O^{2+} toward the channel/GI interface, causing the negative V_{th} shift [5], [9]. Such mechanism is schematically shown in Fig. 11 (c).

As V_O^{2+} migrate, they must overcome the energy barrier E_B. Thus the 2nd-stage NBS is T-activated. In this study, E_B is estimated as the E_a values of 0.13∼0.18 eV for the 2nd-stage degradation (see Table 1), which are close to the reported value of 0.2 eV for ZnO crystals [26]. At higher temperatures, the amount of V_O^{2+} accumulated at the GI/channel interface will increase because the movement of V_O^{2+} will be more active. Therefore, it induces a larger V_{th} shift as the V_{th} shift only depends on the amount of V_O^{2+} accumulated at the interface rather than the total amount of V_O^{2+} in a-IGZO bulk. Under more negative stress V_G, migration of V_O^{2+} towards the interface becomes easier, increasing the negative V_{th} shift.

To understand the slow recovery for negative ΔV_{th} under NBS or NBIS, one should be noted that the formation of V_O^{2+} states is along with a re-arrangement of the neighboring atoms. The required energy barrier for V_O^{2+} returning to neutral V_O is high [25], [26]. It means once the V_O^{2+} states are generated, they can hardly recover, due to such energy barrier.

For the negative V_{th} shift caused by the V_O^{2+}, it holds the relationship between the amount of V_O^{2+} at the interface ΔN_{it} and ΔV_{th}:

$$\Delta V_{\mathrm{th}} = 2q\Delta N_{it}/C_{ox} \tag{4}$$

where C_{ox} is the gate capacitance per unit area. ΔN_{it} is calculated to be 8.0×10^9 cm^{-2} during the 2nd-stage (300-3000 s) NBS degradation for V_G of -20 V at 60 °C.

B. NBIS

For the 1st-stage NBIS degradation, the mechanism is the same as that of the NBS degradation. The reactions described in (2) and (3) will not be affected by a light illumination. Thus the 1st-stage NBIS degradation is basically the same as that of NBS degradation, as supported by the similar C_1 and E_d values for NBS and NBIS degradation (see Table 1).

The 2nd-stage degradation of NBIS can be also attributed to the same V_O^{2+} model. However, an important difference is that the blue light can ionize a large amount of V_O to form V_O^{2+}:

$$V_o \overset{h\nu}{\longleftrightarrow} V_o^{2+} + 2e^- \tag{5}$$

TABLE 2. DOS distribution and extracted parameters.

Parameters	Value	Description
N_C (cm^{-3})	8.0×10^{18}	Effective DOS in CBM
N_V (cm^{-3})	4.5×10^{19}	Effective DOS in VBM
E_g (eV)	3.2	Band-gap
Acceptor-like DOS	$g_A(E) = N_{TA}\, e^{\frac{E-E_C}{kT_{TA}}} + N_{DA}\, e^{\frac{E-E_C}{kT_{DA}}}$	
N_{TA} (eV^{-1} cm^{-3})	1.4×10^{19}	Density of tail states at E=E_C
kT_{TA} (eV)	0.04	Conduction-band-tail slope
N_{DA} (eV^{-1} cm^{-3})	1.5×10^{17}	Density of deep states at E=E_C
kT_{DA} (eV)	0.9	Conduction-band-deep slope
Tail donor-like DOS	$g_{TD}(E) = N_{TD}\exp\ [(E_V - E) / kT_{TD})\ ]$	
N_{TD} (eV^{-1} cm^{-3})	4.5×10^{19}	Density of tail states at E=E_V
kT_{TD} (eV)	0.1	Valence-band-tail slope
Shallow donor-like DOS	$g_{OV}(E) = N_{OV}\exp\ \{-\ [(E - E_{OI}) / W_{OV}]^{\ 2}\}$	
N_{OV} (eV^{-1} cm^{-3})	4.2×10^{16}	Peak of OV states
W_{OV} (eV)	0.1	Mean energy of OV states
E_{OV} (eV)	2.9	Standard deviation of OV states

TABLE 3. The fitted electrons at the interface at different stress time under NBIS with $V_G = -30$ V, $I = 1$ mW/cm^2, $T = 60$ °C.

Stress Time (s)	0	3	10	30	100
Electron concentration (cm^{-3})	0	3.9×10^{10}	5.1×10^{10}	8.0×10^{10}	1.1×10^{11}

since the photon energy of 445 nm light is higher than the energy required for oxygen vacancy ionization ~2.3 eV [23]. In the 2nd-stage NBIS degradation (300-3000 s) with $V_G = -20$ V and $I = 0.6$ mW/cm^2 at 60 °C, calculated V_O^{2+} accumulated at the interface is 2.9×10^{11} cm^{-2}, which is significantly larger than that of NBS degradation under the same V_G and T condition. Hence, the negative V_{th} shift of NBIS is much larger, and the 2nd-stage degradation occurs much earlier than that of the NBS degradation. We could obtain a similar value of E_a for NBS and NBIS even when illumination has ionized a large amount of V_O to form V_O^{2+}. Because for NBS degradation, the amount of V_O^{2+} is also relative a constant because there is always some amount of V_O^{2+} naturally formed in the a-IGZO channel. Under illumination, large amounts of additional V_O^{2+} are generated via photo-excitation rather than thermal excitation. In both cases, thermal generation have little effect on the amount of V_O^{2+} since the thermal energy is too small compared to the required generation energy of 2.3 eV. Thus, the observed E_a of both NBS and NBIS degradation depends on the E_B of the movement of V_O^{2+}. Based on the proposed unified model, degradation of a-IGZO TFTs under negative gate bias stress with or without an illumination can be consistently explained. In fact, the same mechanism is also applicable to PBS and PBIS. It is reported a negative ΔV_{th} for PBS degradation and attributed it to V_O^{2+} defects [27], [28]. In most cases positive shift of V_{th} is reported in PBS degradation of a-IGZO. It suggests that electron trapping is the dominant mechanism in most cases. The positive shift of V_{th} induced by electron trapping overwhelms the negative shift induced by the V_o^{2+} migration.

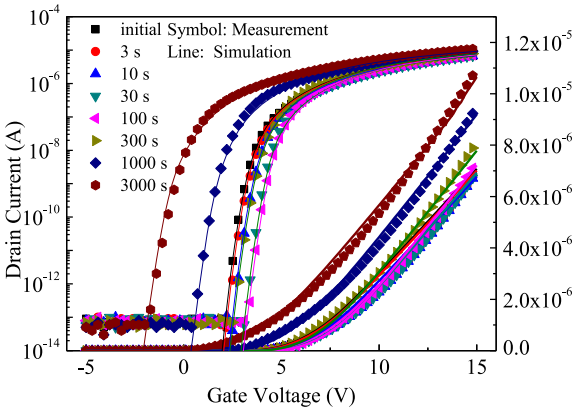

FIGURE 12. Measured and simulated transfer characteristics of the a-IGZO TFT under NBIS for $V_G = -30$ V, $I = 1$ mW/cm^2 in linear and logarithmic scale.

V. TCAD SIMULATION

In this section, simulation of TFT characteristics are made for both 1st- and 2nd-stage degradation by analyzing density of states (DOS) distribution of the subgap states and negative charges for a-IGZO TFTs. Device simulator ATLAS is used to simulate TFT characteristics. To simulate negative charge OH^-, simulation was conducted by putting uniform electrons at the GI/channel interface. By fitting the measured *IV* curves, the subgap DOS and electron amounts are extracted. As is shown in Fig. 12, fitting performance of the TFT *IV* curves shown in Fig. 2 is excellent as seen in both linear and logarithmic scales. To describe DOS profiles of a-IGZO channel, $g_A(E)$ and $g_D(E)$ represent the exponential distribution of acceptor-like and donor-like subgap states, respectively, while $g_{OV}(E)$ represents the Gaussian distribution of donor-like OV states near the conduction band edge (E_C) [29], [30]. Fig. 13 (a) shows the DOS distribution of unstressed a-IGZO TFTs, and related parameters are summarized in Table 2.

To simulate the 1st-stage degradation with $V_G = -30$ V, $I = 1$ mW/cm^2, $T = 60$ °C, the fitted electron amounts increases with stress time as shown in Table 3, while DOS of $g_A(E)$, $g_D(E)$ and $g_{OV}(E)$ remains the same as the initial ones as given in Fig. 13(a). This result verifies that the reason for positive V_{th} shift under NBS and NBIS is the generation of negative charges.

To simulate the 2nd-stage degradation, DOS of $g_A(E)$ and $g_{TD}(E)$ remains the same as the initial ones as given in Fig. 13(a), while $g_{OV}(E)$ near the E_C increases as respectively shown in Fig. 13(b) and (c) for the NBS and NBIS degradation. The increase of $g_{OV}(E)$ can be account for the generation of ionized oxygen vacancies (V_O^{2+}), since the energy level of E_C-0.3eV is consistent with previously reported V_O^{2+} level [23]. This result verifies that the reason for negative V_{th} shift under NBS and NBIS is the generation of V_O^{2+}. On the other hand, the increment of $g_{OV}(E)$ under NBIS is significantly larger than that under NBS, which also corresponds to the fact that the 2nd-stage degradation of NBIS is much more severe than that of NBS. By integrating

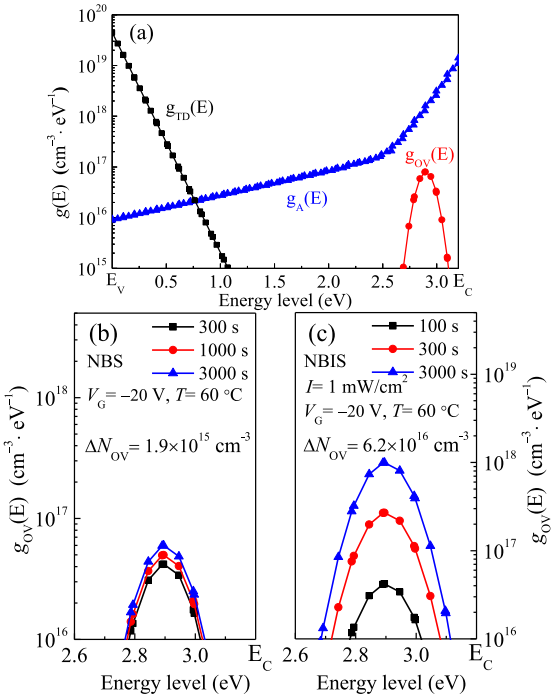

FIGURE 13. (a) Initial DOS distribution of the TFTs. (b) and (c) Extracted distribution of $g_{OV}(E)$ during the second-stage degradation under NBS and NBIS, respectively.

the DOS distribution of $g_{OV}(E)$ shown in Fig. 13(b) and (c), V_O^{2+} density can be calculated for each stress time, from which the increase of the V_O^{2+} density from 300 to 3000 s stress is obtained as 1.9×10^{15} and 6.2×10^{16} cm^{-3} for NBS and NBIS, respectively. Since the channel thickness of a-IGZO is 50 nm, the areal density of V_O^{2+} generation is calculated to be 9.5×10^{9} and 3.1×10^{11} cm^{-2} for NBS and NBIS, respectively, which agree well with the ΔN_{it} values of 8.0×10^{9} and 2.9×10^{11} cm^{-2} calculated by using Eq. (4) for the NBS and NBIS. The agreement is a strong support to the proposed degradation model.

VI. CONCLUSION

In this paper, two distinct degradation behaviors under NBS and NBIS for a-IGZO TFTs were found. One is a two-stage degradation which is a positive V_{th} shift followed by a negative shift, while the other is a continuous negative shift. In both cases, V_{th} shift for NBS and NBIS show similar dependencies on V_G and T, and their recovery processes are also quite similar, which indicates an intrinsic correlation between them. The negative charge OH^- generated at the channel/dielectric interface results in positive V_{th} shift, while V_O^{2+} accumulated at the interface has an opposite effect. On this basis, the NBS and NBIS degradation of a-IGZO TFTs can be understand with the same mechanisms.

ACKNOWLEDGMENT

The authors would like to thank the Kunshan Visionox Technology Co., Ltd., Kunshan, China, for thin-film transistor fabrication.

REFERENCES

[1] K. Nomura, H. Ohta, A. Takagi, T. Kamiya, M. Hirano, and H. Hosono, "Room-temperature fabrication of transparent flexible thin-film transistors using amorphous oxide semiconductors," *Nature*, vol. 432, no. 7016, pp. 488–492, Nov. 2004. doi: 10.1038/nature03090.

[2] T. Kamiya, K. Nomura, and H. Hosono, "Origin of high mobility and low operation voltage of amorphous oxide TFTs: Electronic structure, electron transport, defects and doping," *J. Display Technol.*, vol. 5, no. 7, pp. 273–288, Jul. 2009. doi: 10.1109/JDT.2009.2021582.

[3] M. Delwar, H. Chowdhury, P. Migliorato, and J. Jang, "Light induced instabilities in amorphous indium–gallium–zinc–oxide thin-film transistors," *Appl. Phys. Lett.*, vol. 97, no. 17, Oct. 2010, Art. no. 173506. doi: 10.1063/1.3503971.

[4] S.-Y. Lee *et al.*, "The effect of the photo-induced carriers on the reliability of oxide TFTs under various intensities of light," *IEEE Electron Device Lett.*, vol. 33, no. 2, pp. 218–220, Feb. 2012. doi: 10.1109/LED.2011.2177633.

[5] J. G. Um, M. Mativenga, P. Migliorato, and J. Jang, "Increase of interface and bulk density of states in amorphous-indium-gallium-zinc–oxide thin-film transistors with negative-bias-under-illumination-stress time," *Appl. Phys. Lett.*, vol. 101, no. 11, Sep. 2012, Art. no. 113504. doi: 10.1063/1.4751849.

[6] A. T. Krishnan, V. Reddy, and S. Krishnan, "Impact of charging damage on negative bias temperature instability," in *Proc. IEDM Tech.*, vol. 39, no. 3, Dec. 2001, pp. 1–4. doi: 10.1109/IEDM.2001.979650.

[7] C.-Y. Chen *et al.*, "Negative bias temperature instability in low-temperature polycrystalline silicon thin-film transistors," *IEEE Trans. Electron Devices*, vol. 53, no. 12, pp. 2993–3000, Dec. 2006. doi: 10.1109/TED.2006.885543.

[8] J. Zhou, M. Wang, and M. Wong, "Two-stage degradation of p-channel poly-Si thin-film transistors under dynamic negative bias temperature stress," *IEEE Trans. Electron Devices*, vol. 58, no. 9, pp. 3034–3041, Sep. 2011. doi: 10.1109/TED.2011.2158582.

[9] W.-S. Kim, Y.-H. Lee, Y.-J. Cho, B.-K. Kim, K. T. Park, and O. Kim, "Effect of wavelength and intensity of light on a-InGaZnO TFTs under negative bias illumination stress," *ECS J. Solid-State Sci. Technol.*, vol. 6, no. 1, pp. Q6–Q9, 2017. doi: 10.1149/2.0021701jss.

[10] F.-H. Chen, T.-M. Pan, C.-H. Chen, J.-H. Liu, W.-H. Lin, and P.-H. Chen, "Two-step electrical degradation behavior in α-InGaZnO thin-film transistor under gate-bias stress," *IEEE Electron Device Lett.*, vol. 34, no. 5, pp. 635–637, May 2013. doi: 10.1109/LED.2013.2248115.

[11] R. N. P. Vemuri, W. P. Mathews, M. Marrs, and T. L. Alford, "Investigation of defect generation and annihilation in IGZO TFTs during practical stress conditions: Illumination and electrical bias," *J. Phys. D Appl. Phys.*, vol. 46, no. 4, Jan. 2013. Art. no. 045101. doi: 10.1088/0022-3727/46/4/045101.

[12] J. Bang, S. Matsuishi, and H. Hosono, "Hydrogen anion and subgap states in amorphous In–Ga–Zn–O thin films for TFT applications," *Appl. Phys. Lett.*, vol. 110, no. 23, Jun. 2017, Art. no. 232105. doi: 10.1063/1.4985627.

[13] Y. Nam, H.-O. Kim, S. H. Cho, and S.-H. K. Park, "Effect of hydrogen diffusion in an In–Ga–Zn–O thin film transistor with an aluminum oxide gate insulator on its electrical properties," *Roy. Soc. Chem.*, vol. 8, no. 10, pp. 5622–5628, 2018. doi: 10.1039/c7ra12841j.

[14] R. H. Doremus, "Oxidation of silicon by water and oxygen and diffusion in fused silica," *J. Phys. Chem.*, vol. 80, no. 16, pp. 1773–1775, Jan. 1976. doi: 10.1021/j100557a006.

[15] X. R. Cheng, Y. C. Cheng, and B. Y. Liu, "Nitridation-enhanced conductivity behavior and current transport mechanism in thin thermally nitrided SiO_2," *J. Appl. Phys.*, vol. 63, no. 3, pp. 797–802, 1988. doi: 10.1063/1.340072.

[16] T. P. Chen, S. Li, S. Fung, and K. F. Lo, "Interface trap generation by FN injection under dynamic oxide field stress," *IEEE Trans. Electron Devices*, vol. 45, no. 9, pp. 1920–1926, Sep. 1998. doi: 10.1109/16.711356.

[17] S. Holland, I. C. Chen, T. P. Ma, and C. Hu, "On physical models for gate oxide breakdown," *IEEE Electron Device Lett.*, vol. EDL-5, no. 8, pp. 302–305, Aug. 1984. doi: 10.1109/edl.1984.25925.

[18] X. Lu, M. Wang, and M. Wong, "A two-stage degradation model of p-channel low-temperature poly-Si thin-film transistors under positive bias temperature stress," *IEEE Trans. Electron Devices*, vol. 58, no. 10, pp. 3501–3505, Oct. 2011. doi: 10.1109/TED.2011.2160949.

[19] N. D. Young and A. Gill, "Water-related instability in TFTS formed using deposited gate oxides," *Semicond. Sci. Technol.*, vol. 7, no. 8, pp. 1103–1108, Aug. 1992. doi: 10.1088/0268-1242/7/8/013.

[20] J.-C. Jhu *et al.*, "Investigation of hydration reaction-induced protons transport in etching-stop a-InGaZnO thin-film transistors," *IEEE Electron Device Lett.*, vol. 36, no. 10, pp. 1050–1052, Oct. 2015. doi: 10.1109/LED.2015.2466103.

[21] R. Zhan, C. Dong, P. Liu, and H.-P. D. Shieh, "Influence of channel layer and passivation layer on the stability of amorphous InGaZnO thin film transistors," *Microelectron. Rel.*, vol. 53, no. 12, pp. 1879–1885, 2013. doi: 10.1016/j.microrel.2013.05.007.

[22] M. D. H. Chowdhury *et al.*, "Effect of SiO_2 and SiO_2/SiN_x passivation on the stability of amorphous indium-gallium Zinc–Oxide thin-film transistors under high humidity," *IEEE Trans. Electron Devices*, vol. 62, no. 3, pp. 869–874, Mar. 2015. doi: 10.1109/TED.2015.2392763.

[23] B. Ryu, H.-K. Noh, E.-A. Choi, and K. J. Chang, "O-vacancy as the origin of negative bias illumination stress instability in amorphous In–Ga–Zn–O thin film transistors," *Appl. Phys. Lett.*, vol. 97, no. 2, Jul. 2010, Art. no. 022108. doi: 10.1063/1.3464964.

[24] J. H. Kim, U. K. Kim, Y. J. Chung, and C. S. Hwang, "Correlation of the change in transfer characteristics with the interfacial trap densities of amorphous In–Ga–Zn–O thin film transistors under light illumination," *Appl. Phys. Lett.*, vol. 98, no. 23, Jun. 2011, Art. no. 232102. doi: 10.1063/1.3597299.

[25] K. Ghaffarzadeh *et al.*, "Persistent photoconductivity in Hf–In–Zn–O thin film transistors," *Appl. Phys. Lett.*, vol. 97, no. 14, Oct. 2010, Art. no. 143510. doi: 10.1063/1.3496029.

[26] S. Lany and A. Zunger, "Anion vacancies as a source of persistent photoconductivity in II–VI and chalcopyrite semiconductors," *Phys. Rev. B, Condens. Matter*, vol. 72, no. 3, Jul. 2005, Art. no. 035215. doi: 10.1103/PhysRevB.72.035215.

[27] S. Jin, T.-W. Kim, Y.-G. Seol, M. Mativenga, and J. Jang, "Reduction of positive-bias-stress effects in bulk-accumulation amorphous-InGaZnO TFTs," *IEEE Electron Device Lett.*, vol. 35, no. 5, pp. 560–562, May 2014. doi: 10.1109/LED.2014.2311172.

[28] Y. Yang, D. Zhang, M. Wang, L. Lu, and M. Wong, "Suppressed degradation of elevated-metal metal–oxide thin-film transistors under bipolar gate pulse stress," *IEEE Electron Device Lett.*, vol. 39, no. 5, pp. 707–710, May 2018. doi: 10.1109/LED.2018.2821366.

[29] T. Kamiya, K. Nomura, and H. Hosono, "Origins of high mobility and low operation voltage of amorphous oxide TFTs: Electronic structure, electron transport, defects and doping," *J. Display Technol.*, vol. 5, no. 7, pp. 273–288, Jul. 2009. doi: 10.1109/JDT.2009.2021582.

[30] Y. Kim *et al.* "Amorphous InGaZnO thin-film transistors—Part II: Modeling and simulation of negative bias illumination stress-induced instability," *IEEE Trans. Electron Devices*, vol. 59, no. 10, pp. 2699–2706, Oct. 2012. doi: 10.1109/TED.2012.2208971.